






## RESEARCH ARTICLE OPEN ACCESS

# Elemental Mapping of Historical Daguerreotypes Using Monochromatic Micro-XRF: Imaging, Degradation, and Conservation Potential

Valentina Ljubić Tobisch<sup>1</sup>  | Dieter Ingerle<sup>1</sup>  | Peter Wobrauschek<sup>2</sup>  | Christina Strelj<sup>1,2</sup>  |  
Andreas Steiger-Thirsfeld<sup>3</sup>  | Karin Whitmore<sup>3</sup>  | Wolfgang Kautek<sup>4</sup>  | Klaudia Hradil<sup>1</sup> 

<sup>1</sup>Technische Universität Wien, X-Ray Center, Vienna, Austria | <sup>2</sup>Technische Universität Wien, Atominstytut, Vienna, Austria | <sup>3</sup>Technische Universität Wien, USTEM, Vienna, Austria | <sup>4</sup>University of Vienna, Department of Physical Chemistry, Vienna, Austria

**Correspondence:** Valentina Ljubić Tobisch ([valentina.tobisch@tuwien.ac.at](mailto:valentina.tobisch@tuwien.ac.at)) | Dieter Ingerle ([dieter.ingerle@tuwien.ac.at](mailto:dieter.ingerle@tuwien.ac.at))

**Received:** 17 April 2025 | **Revised:** 27 June 2025 | **Accepted:** 25 July 2025

**Funding:** This work was supported by the PHELETYPIA, “The impact of early photography and electrotyping media on the creation of images and contemporary art” (Heritage 2020-060 PHELETYPIA) in the Heritage Science Austria grant program of the Austrian Academy of Sciences.

**Keywords:** daguerreotype | digital preservation | elemental mapping | heritage science | micro-XRF | SEM/EDS

## ABSTRACT

The daguerreotype, introduced by Louis-Jacques-Mandé Daguerre in 1839, marked the beginning of photography. This early photographic process, based on halide-sensitized silver-coated copper plates developed with mercury vapor, produces highly reflective, image-bearing surfaces that are both visually unique and chemically complex. As part of the interdisciplinary Heritage Science project PHELETYPIA, this study investigates the surface morphology and elemental composition of two historical daguerreotypes from the Varaždin City Museum (Croatia) using monochromatic micro-x-ray fluorescence ( $\mu$ XRF), scanning electron microscopy with energy-dispersive x-ray spectrometry (SEM/EDS), and optical microscopy. By comparing elemental distribution maps based on Hg-L and Au-L lines, we assess the relationship between image particle composition, visual contrast, and degradation patterns. Our results suggest that differences in image formation and preservation are linked to original manufacturing processes, including uneven thermal development and subsequent environmental exposure. High-resolution elemental imaging reveals how visual information is distributed across tonal zones and how it may be affected by previous conservation interventions. These findings highlight the potential of non-invasive analytical imaging to enhance our understanding of daguerreotype image structure, support condition assessment, and inform long-term digital preservation strategies.

## 1 | Introduction

The publication of the photographic process, based on the method developed by Louis-Jacques-Mandé Daguerre [1], on August 19, 1839, is regarded as the birth of photography [2, 3]. The daguerreotype process relied on the photosensitivity of halides Br, Cl, and I, which were applied to a silver-plated copper plate [4–7]. The plate was first polished to a mirror-like finish and then exposed to halogen vapors in a fumigation box. After the exposure was judged to be complete, the image was developed through the

application of heated Hg vapors, after which the plate was fixed with a solution of sodium thiosulfate  $\text{Na}_2\text{S}_2\text{O}_3 \cdot (\text{H}_2\text{O})_x$  to remove any unexposed halides and stop further darkening of the plate [8]. To enhance the image, many daguerreotypes were gilded using gold chloride (AuCl), a treatment that not only increased mechanical stability but also improved visual contrast [9]. Over time, the practice of hand-coloring daguerreotypes also emerged, where powdered pigments were applied manually to the image, providing a vibrant, personalized touch to each daguerreotype [10]. The advancements in photographic chemistry, especially the use of

This is an open access article under the terms of the [Creative Commons Attribution](https://creativecommons.org/licenses/by/4.0/) License, which permits use, distribution and reproduction in any medium, provided the original work is properly cited.

© 2025 The Author(s). *X-Ray Spectrometry* published by John Wiley & Sons Ltd.

more sensitive halogens such as Br and Cl, allowed for substantial reductions in exposure time. This breakthrough enabled the capturing of the first portraits and contributed to the rapid expansion of photographic practices in the 19th century [11–15].

The Heritage Science project PHELETYPIA [16], funded by the Austrian Academy of Sciences, investigates the surface morphology and elemental composition of historical daguerreotypes from museum collections in Austria and other regions of the former Austrian Empire. As part of this project, two 19th-century daguerreotypes (Figure 1) from the Varaždin City Museum, Croatia, were analyzed to examine the spatial distribution of key elements Au, Ag, and Hg using a monochromatic Mo tube-excited micro-x-ray fluorescence spectrometer ( $\mu$ XRF) along with optical microscopy and Scanning Electron Microscopy (SEM) coupled with Energy Dispersive x-ray Spectrometry (EDS). Au, Ag, and Hg play a crucial role in the formation and development of the image on the daguerreotype plate, and understanding their distribution can offer valuable insights into the photographic process as well as the subsequent degradation of the image [17–20]. While applications of microbeam imaging techniques on daguerreotypes have been previously tested using synchrotron radiation, this work compares two different sets of results, with Hg-L and Au-L as the main imaging sources [21]. By comparing these two imaging modalities, we aim to better understand how elemental distributions contribute to image formation and how these are shaped by variations in the original manufacturing process.

In addition to investigating degradation phenomena, this study aims to identify where exactly the visual information is preserved on the daguerreotype surface and whether differences in image particle distribution may be linked to the specific manufacturing technique used. Within the museum sector as well as among private collectors, there is growing caution toward cleaning methods due to the risk of irreversible damage to these sensitive photographic objects [4, 22].

Furthermore, historical daguerreotypes often exhibit traces of earlier polishing or cleaning interventions which, although sometimes intended as preservation measures, may have unintentionally affected the image layer. While mechanical polishing is discouraged under modern conservation ethics, past treatments may have changed the surface microstructure. Non-professional or unmonitored cleaning procedures or handling are known to initiate uncontrolled surface corrosion and can

result in a loss of image particles—both in highlight and shadow regions [23–29]. While image particles are also characterized in scientific literature through their distribution across tonal areas [4, 5, 21], such evaluations are not feasible during routine conservation treatments. In practice, cleaning outcomes are typically judged based on surface brightness [22], making potential losses of image information difficult to detect with the naked eye. Yet these particles are essential for both visual perception and analytical interpretation of daguerreotypes. Losses that go unnoticed during cleaning can still significantly affect the long-term readability and authenticity of the image.

As a result, non-invasive imaging techniques such as elemental mapping offer a promising alternative for gaining insights into both the chemical and morphological structure of daguerreotype images. High-resolution surface analyses not only deepen our understanding of image formation and degradation processes but also provide a foundation for the development of digital preservation strategies. These approaches are entirely contactless and do not alter the original object, while enabling the long-term retention of image-related information—even as the visual clarity of the plate continues to diminish due to ongoing tarnishing and corrosion [30–32].

To better understand how a daguerreotype image forms and evolves over time, it is essential to consider both its microstructure and chemical composition. The visual impression of the daguerreotype arises from the interplay between specular and diffuse reflectance across the image surface. Highlight areas consistently appear bright due to their high reflectivity, while the appearance of shadow regions can change depending on the viewing angle and lighting conditions.

The final appearance of the image is influenced not only by the original processing techniques but also by subsequent aging processes. The alteration of daguerreotypes upon unframing is often characterized by the emergence of previously concealed degradation patterns, such as tarnish, corrosion, or fading [18, 24, 33–36]. These changes are typically a result of differential exposure to environmental conditions such as humidity or pollutants, caused by the protective, yet microclimate-altering effects of the original framing materials. However, it is important to note that some of the peripheral tarnish layers commonly observed after unframing may not solely result from environmental exposure but may also originate from manufacturing-related factors, such as uneven halide sensitization or incomplete development near the edges. In such cases, these early-process-induced vulnerabilities can serve as initiation sites for corrosion, which are then progressively exacerbated by long-term environmental influences [4, 20]. This phenomenon is clearly observable on two unframed daguerreotypes from the Varaždin City Museum, Croatia (Figure 3). In both cases, edge-related corrosion and discoloration patterns reveal the extent of environmental impact previously masked by the frame. Additionally, a significant difference in contrast and tonal range between the two images is visible, particularly in the facial areas. These visual discrepancies are likely related to differences in original processing, image particle morphology, and/or degradation phenomena. Therefore, the characterization using optical microscopy, SEM/EDS, and  $\mu$ XRF is essential to better understand the underlying chemical and morphological features contributing to the observed variations.



**FIGURE 1** | Framed daguerreotypes, Varaždin City Museum, Croatia. (a) Felix Jaccomini with his parents, around 1845, (GMV 77403); (b) Portrait of a boy, around 1850 (GMV 77405). [Colour figure can be viewed at [wileyonlinelibrary.com](https://onlinelibrary.wiley.com)]

Recent work by Kozachuk et al. has demonstrated the potential of synchrotron-based  $\mu$ -XRF mapping, particularly of the Hg L lines, for visualizing heavily tarnished 19th-century daguerreotypes [21]. This approach enables high-resolution chemical imaging, revealing even fine structural details of the original image, such as textile folds or ornamental furniture, based solely on the distribution of Hg residues. The use of L-line emission is preferred due to the greater energy separation between Hg and Au lines, facilitating spectral deconvolution and reducing interference from the Cu bulk material. Additionally, synchrotron analyses were shown to induce no observable changes to the optical appearance or chemical stability of the daguerreotypes, which is a critical consideration for conservation applications.

Earlier works by Davis et al. utilized  $\mu$ -XRF imaging and high-resolution x-ray absorption near-edge structure (HR-XANES) to investigate the distribution of Hg and Au in 19th-century daguerreotypes [17, 19]. Their study employed a laboratory system to collect M-line fluorescence and succeeded in producing elemental images of plates that were largely intact and exhibited minimal tarnish. However, the limited energy separation between the Au and Hg M-lines posed challenges for signal differentiation, particularly in the presence of strong background signals from the Cu bulk material. In contrast, the use of L-line emission offers better spectral resolution and is more suitable for imaging highly corroded daguerreotypes.

While the advantages of synchrotron radiation in terms of spatial resolution, signal quality, and tunability are well recognized, access to such facilities remains limited, particularly for museum-held cultural heritage objects. In the context of the Heritage Science project PHELETYPIA [16], which focuses on the non-destructive analysis of daguerreotypes from museum collections, several practical constraints must be considered. These include legal limitations on the international transport of heritage items, institutional loan policies, and the requirement for continuous oversight by museum staff or conservators during handling and analysis. Furthermore, loan durations are typically restricted, and interventions such as test cleaning cannot be carried out.

Consequently, this study explores the potential of laboratory-based  $\mu$ -XRF system, in combination with SEM/EDS and optical microscopy, as accessible, non-invasive alternatives for in situ analysis of daguerreotypes. Although these systems may not achieve the same level of resolution as synchrotron, they offer a viable solution for heritage institutions aiming to investigate and preserve these delicate photographic materials within the constraints of conservation practice.

## 2 | Materials and Methods

### 2.1 | Historical Daguerreotypes

For this study, two daguerreotypes from the collection of the Varaždin City Museum in Croatia were examined (Figure 1). The first daguerreotype, dating to around 1845, depicts Felix Jaccomini with his parents and measures 65×85 mm (Figure 1a). The unknown photographer captured a young man in a dark suit with a light waistcoat, seated beside a woman in a light-colored dress with a Biedermeier frieze hairstyle. Next to her is a mustachioed man

in a dark suit. The daguerreotype is mounted on yellowish cardboard and housed in a pressed brass frame. The second daguerreotype, from around 1850, features a portrait of a young boy dressed in a coat and striped trousers, with a plate size of 80×70 mm (Figure 1b). He is seated sideways in a chair with a decorative backrest. The image is framed with decorated vignettes and a cardboard mount, indicating a common mid-19th-century framing practice.

### 2.2 | Optical Microscopy

The optical properties of the daguerreotypes were examined using a Keyence VHX-7000 digital microscope.

### 2.3 | SEM/EDS

Further surface characterization was performed using Scanning Electron Microscopy (SEM) coupled with Energy Dispersive x-ray Spectrometry (EDS). EDS is an analytical technique used to identify the elemental composition of materials. It works by detecting the x-rays emitted from a sample when it is bombarded with high-energy electrons in an SEM. These electrons interact with the atoms in the sample, exciting them and causing the emission of characteristic x-rays. Each element emits x-rays at specific energy levels, allowing for qualitative and semi-quantitative analysis of the sample's elemental composition.

The EDS system captures these x-rays and produces a spectrum, where the peaks correspond to the elements in the sample, and the intensity of the peaks reflects the concentration of each element in the excited measuring volume. While the elemental identification is normally easy to perform, problems arise during quantification, especially when there is a severe overlap of peaks of major constituents, with minor constituents close to the detection limit of the method.

The SEM used was a Thermo Fisher Quanta FEG 250, while the EDS measurements were performed using an AMETEK EDAX Octane Elite Super detector with a DDP4 analyser. All measurements were performed with an electron beam current of 1 nA and a beam energy of 10–20 keV. The recording time of the spectra was 30 live seconds. Different acceleration voltages were used for SEM imaging: 10 kV to achieve high-resolution, surface-sensitive imaging of the fragile image layer, and higher voltages of 20 kV for EDX analysis to enable reliable excitation of the characteristic x-rays of heavier elements such as Ag, Au, and Hg [37].

### 2.4 | Micro XRF

Elemental imaging of the sample surface was further conducted using micro-x-ray fluorescence ( $\mu$ XRF). This non-destructive, 2D elemental imaging analytical technique is based on the emission of element characteristic x-rays after irradiation by x-rays from specific points. The fluorescence radiation is measured by an energy dispersive detector, allowing for the simultaneous measurement of the fluorescence radiation from a large number of elements in a sample. Monochromatic excitation was used as it provides better background conditions, especially in the energy range of Au and Hg-L lines. Details can be found in ref [38].

In comparison to standard XRF,  $\mu$ XRF is based on a micro beam scanning the sample and allows elemental imaging. The spatial resolution is given by the size of the x-ray beam ( $\mu\text{m}$  range).

The micro-XRF spectrometer used for the analysis of the Daguerreotypes was a custom-made monochromatic setup [38] (Figure 2). The source assembly consists of a water-cooled fine-focus x-ray diffraction tube and a parallel beam mirror, which produces a quasi-parallel, monochromatic beam. The presented results were obtained using a 2 kW molybdenum tube and a mirror for Mo- $K\alpha$ . The setup itself consists of a polycapillary half lens with a focus size of  $\sim 15\mu\text{m}$  for Mo- $K\alpha$ . A 50 mm [2] silicon drift detector is mounted. Detection limits for e.g., As (10.5 keV) in a glass-certified reference material NIST 621 are in the range of  $1\mu\text{g/g}$ . Details of the specifications of the setup and detection limits can be found in ref [38]. For this specific task, the focal spot was too small, so the scans have been performed out of the focus to provide a spot size of about  $50\mu\text{m}$ . The tube was operated with 50 kV and 40 mA,  $50\mu\text{m}$  spot/step size, 10 s per point

measuring time. All spectra were fitted with the deconvolution software PyMCA [39].

A special holder pressing the metal plate only from the side with an adjustable distance of the plugs was designed and realized by a 3D printer. The size of the  $\mu$ XRF images can be seen in Figures 9 and 12,  $30\times 12\text{mm}$  and  $20\times 20\text{mm}$  respectively. The total scan time was 14 days per image (Figure 3).

### 3 | Results and Discussion

#### 3.1 | Two Case Studies: Felix Jaccomini With His Parents & Portrait of a Boy

The daguerreotype image resides at the very surface of the plate, forming a delicate relief composed of image particles distributed across a highly polished silver surface. These nanostructures vary in size, shape, and spatial distribution

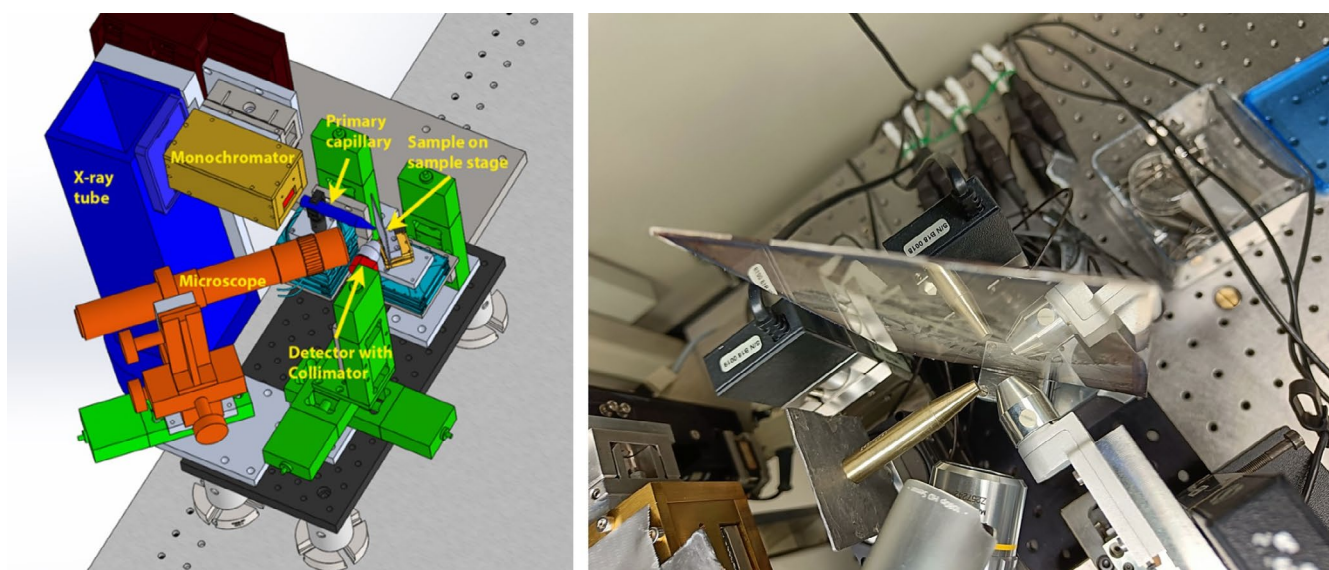


**FIGURE 2** | Setup of the micro-XRF spectrometer including the daguerreotype sample in position. [Colour figure can be viewed at [wileyonlinelibrary.com](https://onlinelibrary.wiley.com)]



**FIGURE 3** | Unframed daguerreotypes, Varaždin City Museum. (a) Croatia Felix Jaccomini with his parents, around 1845, (GMV 77403), (b) portrait of a boy, around 1850 (GMV 77405). Edge-related corrosion and discoloration patterns are clearly visible following removal from the frame. [Colour figure can be viewed at [wileyonlinelibrary.com](https://onlinelibrary.wiley.com)]

depending on their location within the image. In the highlight areas, the particle concentration is highest. Here, the particles are often small and may appear nearly spherical, although irregular shapes resembling “potato-like” forms are also observed. In midtone areas, the particles are generally larger, more irregular in shape, and less densely distributed. Shadow areas contain few or no image particles; those present tend to be larger and form irregular agglomerates, sometimes referred to—following Barger’s terminology—as—“shadow-particle agglomerates” [5]. The structural characteristics of image particles in various tonal regions of the daguerreotype are illustrated in Figure 4, which shows SEM analyses of the portrait Felix Jacomini with his parents (ca. 1845, GMV 77403), including particle size distributions in shadow, midtone, and highlight areas. Particle size distributions vary systematically across tonal zones: in the shadow region, particles range from 560 to 2250 nm in diameter; in the midtone region, from 340 to 1900 nm; and in the highlight region, from 240 to 600 nm. All SEM images were acquired at 10 keV in high vacuum mode at 80,000 $\times$  magnification. These results are consistent with previous literature, which also reports a correlation between tonal regions and particle size distributions, with smaller, more densely packed particles in highlight areas and larger, more irregular agglomerates in shadow zones.

Figure 5a shows an SEM image of a highlight region, the white shirt region from the father of Felix Jacomini. A large number of image particles of different sizes can be recognized. EDS analysis revealed that Hg is concentrated in the larger or agglomerated image particles (Selected Area 2). No increased Hg content was detected in areas with separated small image particles (Selected Area 1). The measured areas contain approximately the same amount of Au (Figure 5b).

In a shadow region, the black suit waistcoat region from the father of Felix Jacomini, in addition to the few small image particles, individual large ones can be recognized, see Figure 6a.

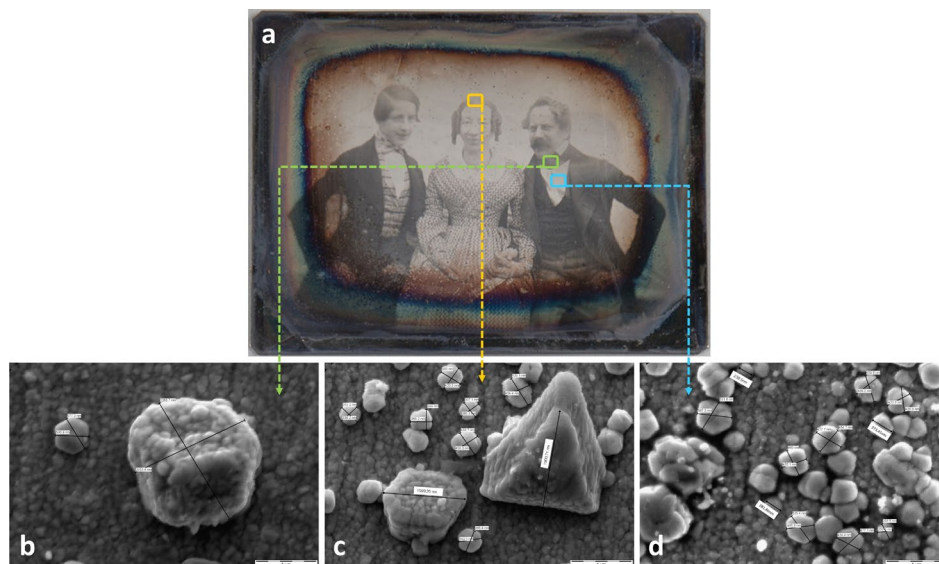
Hg is enriched in the large image particles (Selected Area 1 and Selected Area 2) as in the exposed region; again, the amount of Au is approximately the same in the measured areas.

Figure 7a shows an SEM image of a highlighted region, the shirt collar, from the boy’s portrait. Numerous image particles are recognizable, compared to the shadow region (Figure 7b), the chair back, where only a few image particles are visible. The color-framed areas in the images correspond to the measurement regions. The names of the measuring regions, the resulting spectra, and the results of the corresponding quantitative analysis are shown in the same colors.

The chemical analysis of the two large areas, Selected Area 1 in the exposed region and Selected Area 2 in the unexposed region, shows little difference; the amount of Au is the same, and a small amount of Hg is present in the highlight region. A spot measurement (EDS point 1) on a conglomerate of image particles in the highlight region indicates higher amounts of Hg and Au. The chemical analysis shows that especially Hg used for development and, to a smaller extent, Au used for image enhancement, preferentially accumulate on the image particles. Na is measured in both regions, which is indicative of cover glass corrosion, most likely resulting from ion exchange processes associated with long-term environmental exposure (Figure 7c) [39].

Due to the strong overlap of the peaks with Ag and Hg, the elements Cl and S cannot be verified with certainty. This problem occurs in all EDS measurements done on these samples.

The main difference between  $\mu$ XRF and SEM/EDS is the excitation with monochromatic Mo-K $\alpha$  leading to a penetration depth for Mo-K $\alpha$  in Ag  $\sim$ 30–35  $\mu$ m, which is much deeper than with electrons. Therefore, the Cu-K lines from the Cu bulk material below the Ag layer are visible in the spectrum. The advantage of excitation with Mo-K $\alpha$  (17.4 keV) lies in a better excitation of Au-L and Hg-L lines, which are better separable than the corresponding



**FIGURE 4** | SEM analysis of different tonal areas of the daguerreotype Felix Jacomini with his parents, ca. 1845, (GMV 77403), Varaždin City Museum, Croatia. (a) Unframed daguerreotype with marked positions for SEM imaging: Green = shadow area (b), yellow = midtone (c), blue = highlight (d); (b) Shadow region: Particle diameters 560–2250 nm; (c) Midtone region: 340–1900 nm; (d) Highlight region: 240–600 nm. All SEM images acquired at 10 keV in HV mode and 80,000 $\times$  magnification. [Colour figure can be viewed at [wileyonlinelibrary.com](https://onlinelibrary.wiley.com)]

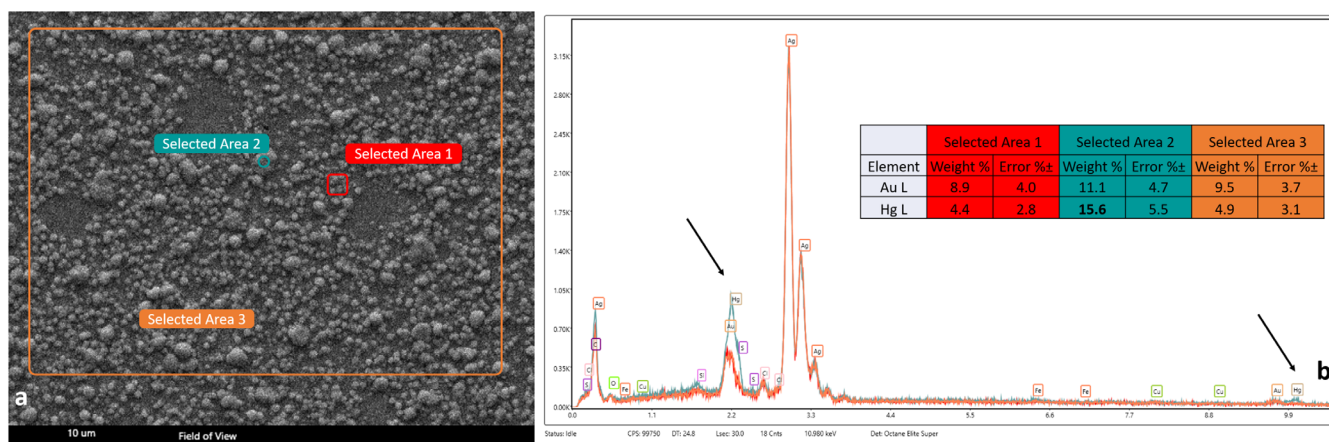


**FIGURE 5** | SEM/EDS analysis of a highlight region (father's white shirt) in GMV 77403. (a) SEM image showing large and agglomerated image particles (Selected Area 1) as well as smaller dispersed particles (Selected Area 2); (b) corresponding EDS spectra with the concentration of Hg, and Au in weight %, for the respective measurements. [Colour figure can be viewed at [wileyonlinelibrary.com](https://onlinelibrary.wiley.com)]

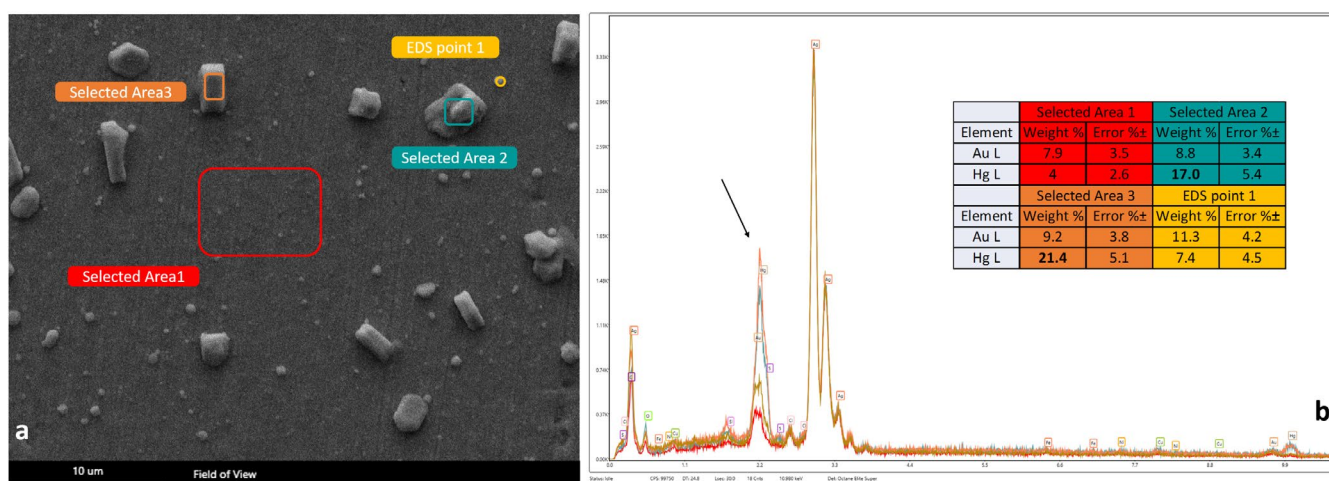


**FIGURE 6** | SEM/EDS analysis of a shadow region (father's dark waistcoat) in GMV 77403. (a) SEM image showing scattered small particles and individual large particles; (b) EDS spectra with the concentration of Hg, and Au in weight %, for the respective measurements. [Colour figure can be viewed at [wileyonlinelibrary.com](https://onlinelibrary.wiley.com)]

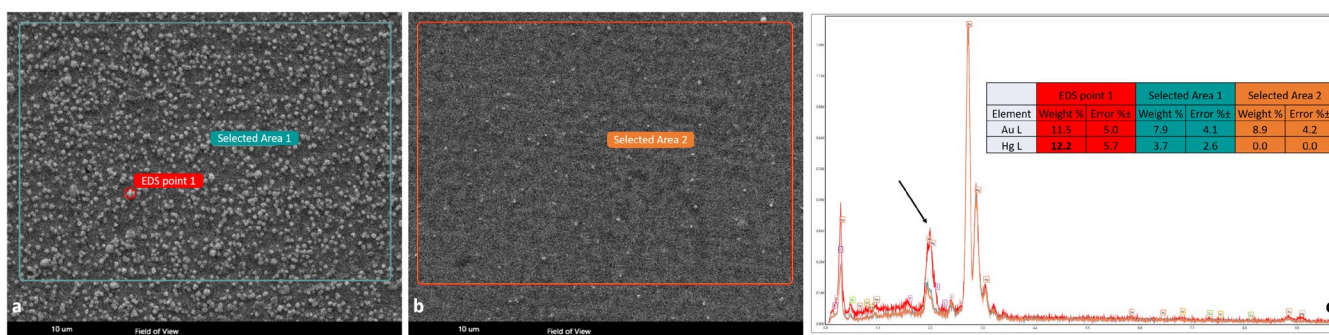


**FIGURE 7** | SEM/EDS analysis of highlight and shadow regions in GMV 77405. (a) Boy's shirt collar with numerous image particles; (b) Chair back showing fewer particles; (c) EDS spectra for Selected Areas 1 and 2, revealing higher Hg and Au content in image particle conglomerates. [Colour figure can be viewed at [wileyonlinelibrary.com](https://onlinelibrary.wiley.com)]

M-lines used for the SEM/EDS. Figure 8 shows the summed spectrum of GMV77403, obtained by integrating data from all individual spectra recorded during the scan. The elements Cu, Ag, Au, Hg, and Pb were detected. The signal intensities of Au and Hg appear to be of comparable magnitude.

In Figure 9, the Au map reveals certain features of the original image more clearly than the Hg map. Notably, in the central area, the intricate lace collar worn by the mother becomes visible in the Au distribution, while it is barely discernible in the Hg map. Additionally, the folds and ripples in the fabric background

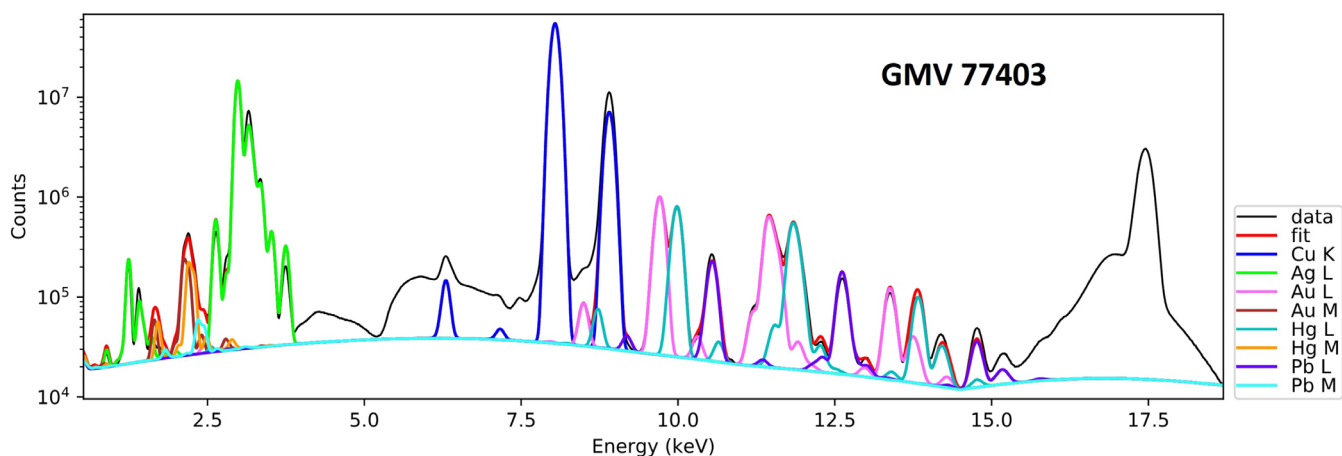


**FIGURE 8** | Summed  $\mu$ XRF spectrum of GMV 77403. Peak deconvolution performed using PyMCA [38]. [Colour figure can be viewed at [wileyonlinelibrary.com](https://onlinelibrary.wiley.com)]

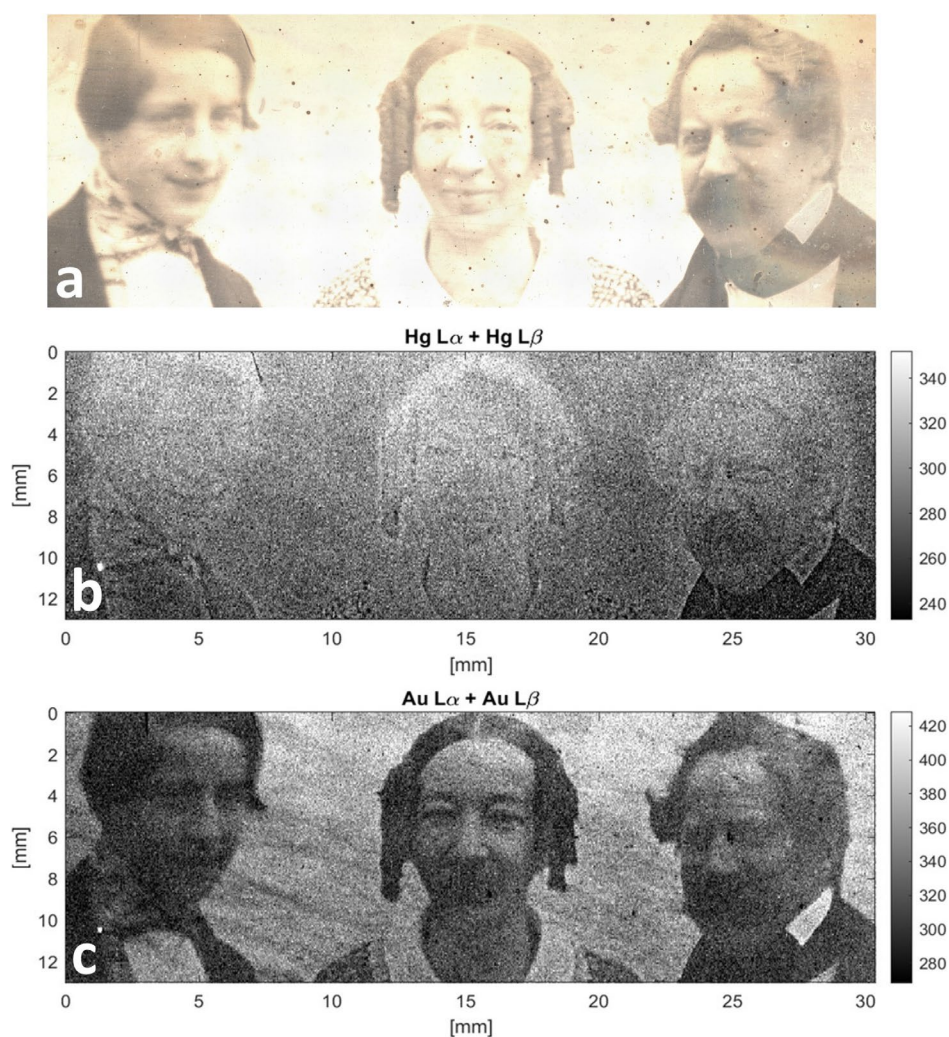


**FIGURE 9** | Felix Jaccomini with his parents, GMV 77403. (a) Optical micrograph of the central area, highlighting the faded region in the middle of the plate; (b)  $\mu$ XRF elemental distribution map of mercury (Hg  $L\alpha$  and  $L\beta$  lines); (c)  $\mu$ XRF elemental distribution map of gold (Au  $L\alpha$  and  $L\beta$  lines). [Colour figure can be viewed at [wileyonlinelibrary.com](https://onlinelibrary.wiley.com)]

are more distinctly resolved in the Au map. In contrast, facial features such as eyes and mouths appear strongly faded in both elemental maps and show very little contrast. The Hg signal

intensity increases toward the father's collar and downward, suggesting a lower concentration of Hg in the facial regions. This variation could be attributed either to a reduced amount

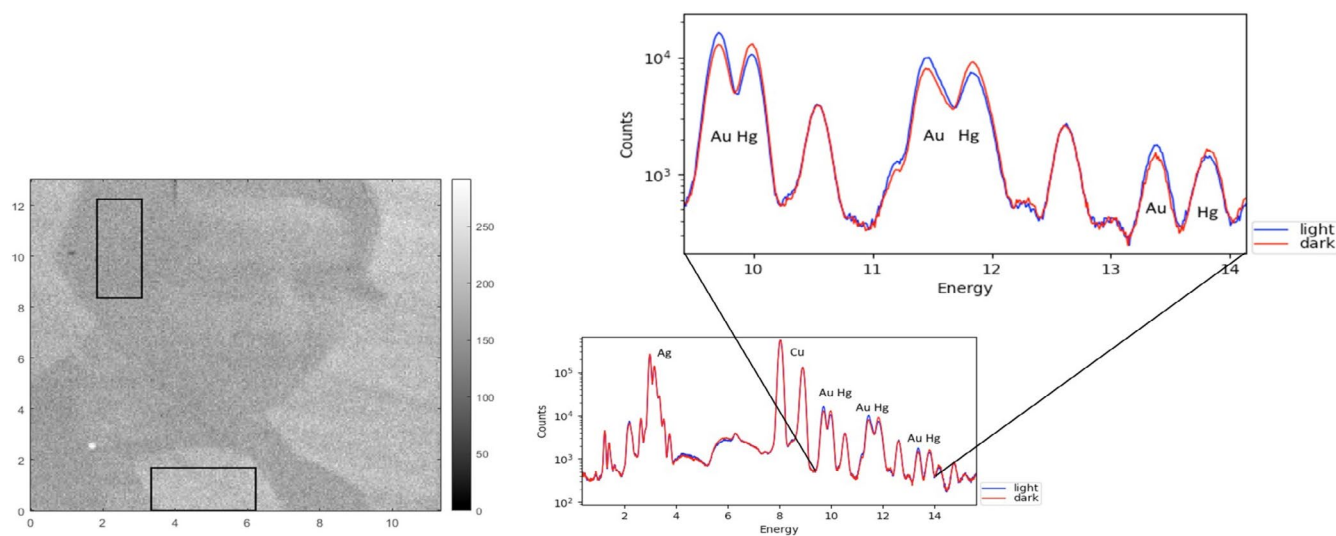
of Hg or to an incomplete development process in these areas. Another possible explanation is local overheating of the plate during development, which may have led to insufficient Hg condensation on the exposed Ag surface. While standard Hg boxes ensured relatively even heating, typically using a spirit lamp at a controlled distance, some daguerreotypists may have used improvised or self-built development setups, potentially introducing local thermal variations across the plate [4].

To investigate potential differences in the Au/Hg ratio between light and dark image areas, 1400 spectra were summed from the dark hair region and another 1400 from the light shirt area of Felix Jacomini in GMV 77403. The resulting spectra are shown in Figure 10. While the signal intensities of Ag and Cu remain consistent across both regions, a clear difference is observed in the distribution of Au and Hg: the dark area exhibits a higher concentration of Hg and a lower concentration of Au, whereas in the light area, Au dominates over Hg. This variation is particularly evident in the extracted L-line regions of the summed

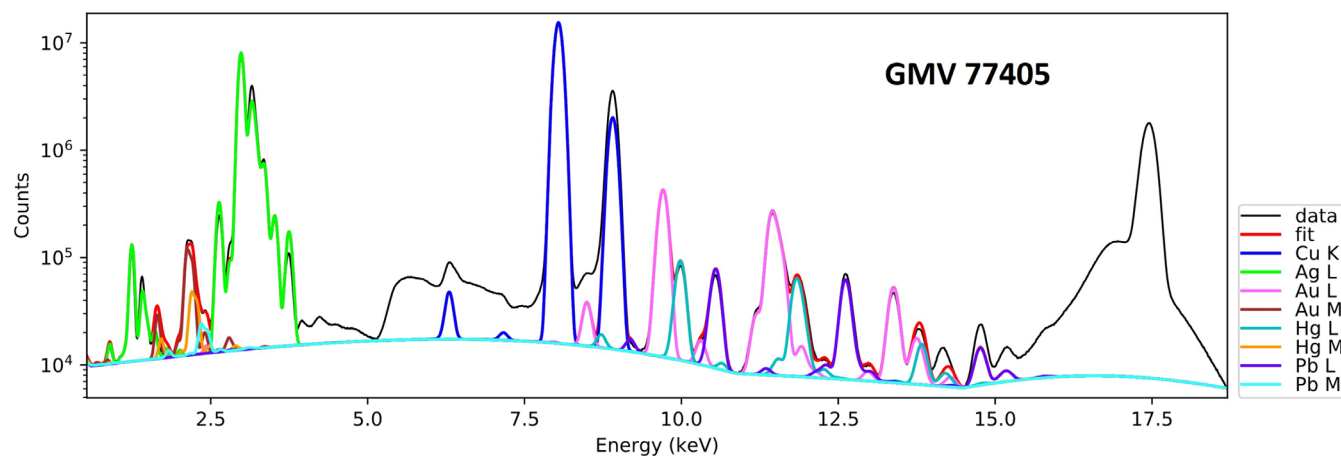
spectra and may reflect localized differences in the development process or material deposition.

Figure 11 shows the summed spectrum of GMV 77405 (Portrait of a boy), obtained by integrating all individual spectra recorded during the  $\mu$ XRF scan. The detected elements include Cu, Ag, Au, Hg, and Pb. In this spectrum, the signal intensity of Au is approximately 50% higher than that of Hg. This contrasts with the summed spectrum of GMV 77403 (Felix Jacomini with his parents), shown in Figure 8, where the signal intensities of Au and Hg are comparable.

The elemental distribution maps of Au-L and Hg-L for GMV 77405 (Portrait of a boy) are shown in Figure 12. In this case, the Hg map reveals significantly more image detail than the Au map. Notably, the ripples in the boy's hair—barely visible in the optical micrograph—are distinctly resolved in the Hg distribution. In addition, the overall contrast of facial contours, including fine facial features such as the boy's intense



**FIGURE 10** |  $\mu$ XRF scan of GMV 77403 indicating the regions analyzed for spectral comparison: dark hair area and light shirt area (left); overlap of the sum spectra of the dark (red) and the light (blue) area with an extraction of the area of the Au and Hg L $\alpha$ , L $\beta$  and L $\gamma$  lines (right). [Colour figure can be viewed at [wileyonlinelibrary.com](https://onlinelibrary.wiley.com)]



**FIGURE 11** | Summed  $\mu$ XRF spectrum of GMV 77405. Peak deconvolution performed using PyMCA [38]. Au signal is  $\sim$ 50% higher than Hg, contrasting with the spectrum of GMV 77403. [Colour figure can be viewed at [wileyonlinelibrary.com](https://onlinelibrary.wiley.com)]

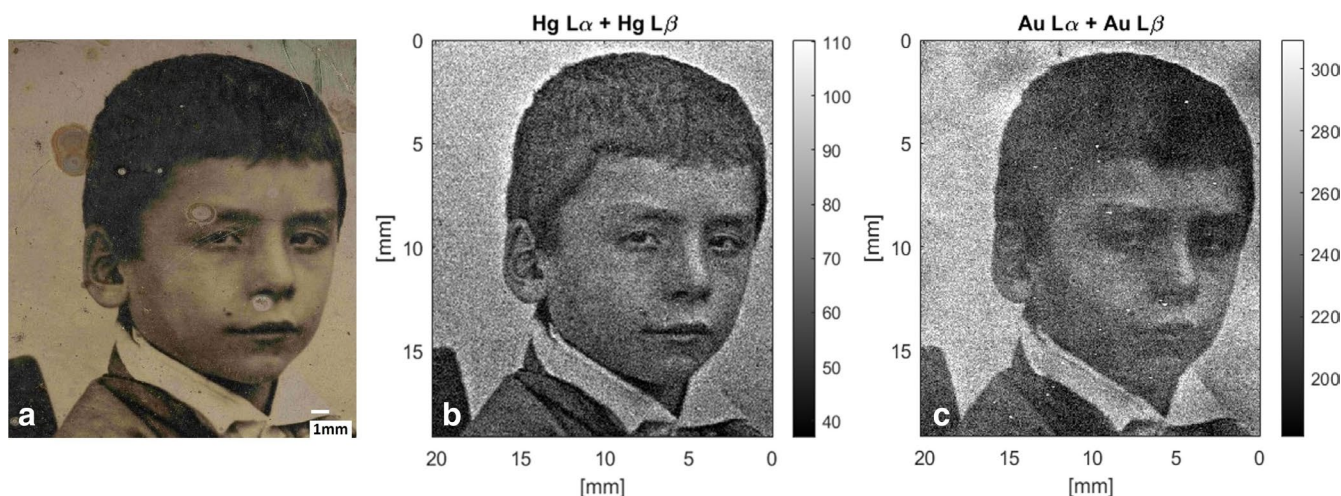


**FIGURE 12** | Portrait of a boy, GMV 77405. (a) Optical micrograph; (b)  $\mu$ XRF elemental distribution map of Hg (Hg L $\alpha$  and L $\beta$ ); (c) elemental distribution map of Au (Au L $\alpha$  and L $\beta$ ). The Hg map provides higher image detail, especially in hair texture, than the Au or optical image. [Colour figure can be viewed at [wileyonlinelibrary.com](https://onlinelibrary.wiley.com/doi/10.1002/ami.2021.01082)]

gaze and the details of his clothing in the lower part of the image, are more clearly rendered in the Hg scan. This stands in contrast to the findings for GMV 77403, where the Au map provided better visual definition. Interestingly, the prominent corrosion spots visible on the daguerreotype plate are not apparent in either the Au or Hg elemental maps, suggesting that these surface defects do not significantly affect the distribution of image-forming elements or their detectability through  $\mu$ XRF imaging.

Another research question addressed in this study was the detection of halogens, particularly Cl and Br, as their presence could offer insights into the original photographic processing techniques. However, significant limitations arise when attempting to analyze halogens using energy-dispersive x-ray fluorescence (EDXRF) in the presence of Ag, Au, and Hg.

In the case of chlorine, the Cl K $\alpha$  line at 2.62 keV overlaps with the Ag L $\ell$  line at 2.63 keV. This spectral interference makes it impossible to reliably resolve the Cl signal, even with advanced deconvolution software, when Ag is present in significantly higher concentrations. A comparable problem occurs with bromine: the Br K-L $_2$  (11.88 keV) and Br K-L $_3$  (11.92 keV) lines overlap with the Hg L $_2$ -M $_4$  (11.82 keV) and Au L $_3$ -O $_1$  (11.91 keV) lines, respectively.

We therefore conclude that, under these conditions, the detection of Cl and Br using energy-dispersive XRF is not feasible due to fundamental spectral overlaps with major constituent elements.

## 4 | Conclusions

This study provides new insights into the complex surface chemistry and image structure of historical daguerreotypes through the application of non-invasive, high-resolution analytical techniques. By combining monochromatic micro-XRF, SEM/EDS, and optical microscopy, the image-forming particles were characterized with respect to their size, distribution, and elemental

composition in various tonal zones of two 19th-century daguerreotypes from the Varaždin City Museum, Croatia.

The findings indicate that the visual appearance of daguerreotypes is not only shaped by the original photographic chemistry, but also by the thermal conditions during the development process. Uneven heating during mercury vapor development likely contributed to heterogeneities in particle formation, particularly the presence of larger, Hg-rich agglomerates in otherwise fine-grained highlight regions. These inconsistencies are associated with reduced image contrast, localized fading, and a loss of fine detail—phenomena that were clearly observable in both visual inspection and elemental distribution maps.

Moreover, the study reveals that Hg and Au are not evenly distributed across the image surface, and their relative intensities vary significantly between light and dark image areas. In some cases, the Au-L maps provided better visual definition of textile features and ornamental structures, while Hg-L maps highlighted facial details or hair textures, underscoring the complementary nature of these imaging modalities. This nuanced behavior of elemental contrast provides valuable diagnostic information for understanding both image formation and degradation mechanisms.

This study emphasizes the importance of non-invasive imaging techniques in the assessment of daguerreotypes, both for scientific research and for the development of conservation protocols. By documenting the distribution of image-forming elements and correlating them with visual and structural changes, these methods allow for more informed decisions regarding treatment, handling, and digital preservation. Given the fragility and historical value of daguerreotypes, such approaches offer a critical means of safeguarding both material integrity and visual information for future generations.

Finally, the findings highlight methodological limitations in detecting halogen residues (Cl, Br, I) due to spectral overlaps in energy-dispersive XRF analysis. This calls for further refinement of detection strategies, possibly involving synchrotron-based or

wavelength-dispersive techniques, particularly in studies seeking to reconstruct original photographic recipes or investigate regional production methods in early photography.

## Acknowledgments

N/A

## Conflicts of Interest

The authors declare no conflicts of interest.

## Data Availability Statement

The data that support the findings of this study are available from the corresponding author upon reasonable request.

## References

1. L. J. M. Daguerre, *Historique et Description Des Procédes Du Daguerreotype et Du Diormama* (Delloye Libraire, 1839).
2. J. M. Eder, *Geschichte Der Photographie*, vol. 1 (Halle, 1932).
3. J. M. Eder, *History of Photography* (Dover Publications, Inc, 1978).
4. M. S. Barger and W. B. White, *The Daguerreotype: Nineteenth-Century Technology and Modern Science* (Johns Hopkins University Press, 2000).
5. M. S. Barger, "Robert Cornelius and the Science of Daguerreotypy," in *Robert Cornelius. Portraits From the Dawn of Photography*, ed. W. F. Stapp (Smithsonian Institution Press, 1983), 111–128.
6. V. Ljubić Tobisch and W. Kautek, "Highly Photosensitive Daguerreotypes and Their Reproduction: Physico-Chemical Elucidation of Innovative Processes in Photography Developed Around 1840 in Vienna," *ChemPlusChem* 84 (2019): 1730–1738.
7. H. L. Fizeau, "Fizeau, über den Gebrauch des Broms bei der Photographie auf Plaqué," *Polytechnic Journal* 81 (1841): 365–366.
8. Berkeley & King, E. F, *The Literary Gazette and Journal of Belles Lettres Arts Sciences*, vol. 1231 (Oxford University, 1840), 545.
9. Research on the Gilding of Daguerreotypes, *The Daguerreian Society Symposium* (The Daguerreian Society, 2014).
10. M. S. Kozachuk, M. O. Avilés, R. R. Martin, B. Potts, T. K. Sham, and F. Lagugné-Labarthe, "Imaging the Surface of a Hand-Colored 19th Century Daguerreotype," *Applied Spectroscopy* 72 (2018): 1215–1224.
11. G. A. Wickliff, "Light Writing: Technology Transfer and Photography to 1845," *Technical Communication Quarterly* 15 (2006): 293–313.
12. P. Trnkova, "The Beginnings of Photography in Central Europe: Friedrich Franz and the First Daguerreotypes in Brno," *History of Photography* 39 (2015): 121–141.
13. T. Vitale, "Brief History of Imaging Technology," 2013, <https://cool.culturalheritage.org/albumen/>.
14. S. K. Gillespie, *The Early American Daguerreotype* (MIT Press, 2016).
15. C. Kemp, "LICHT-BILD-EXPERIMENT. Franz von Kobell, Carl August Steinheil und die Erfindung der Fotografie in München," *Deutsches Museum Abhandlungen Und Berichte* 27 (2024): 368.
16. V. Ljubić Tobisch, A. Artaker, and W. Kautek, "PHELETYPIA," in *Project PHELETYPIA The Impact of Early Photography and Electrotyping Media on the Creation of Images and Contemporary Art* (Heritage 2020-060 PHELETYPIA by the Heritage Science Austria Grant Program of the Austrian Academy of Sciences, 2023).
17. J. M. Davis, C. Hilton, and E. P. Vicenzi, "Micro XRF Imaging of Daguerreotypes," *Microscopy and Microanalysis* 20, no. 1–2 (2014): 2028–2029.
18. M. Robinson and E. P. Vicenzi, "A Twin Paradox: A Study of Preservation and Disfigurement of Southworth and Hawes Daguerreotypes," *Topics in Photographic Preservation* 16 (2015): 187–205.
19. J. M. Davis and E. P. Vicenzi, "Optimizing Compositional Images of Daguerreotype Photographs Using Post Processing Methods," *Heritage Science* 4 (2016): 14.
20. E. P. Vicenzi, T. Lam, R. Wetzel, and S. T. Perich, "A Nondestructive Method for Probing Layer Thicknesses in Early Photographs From Micrometers to Nanometers Using SEM-Based XRF Spectrometry A Nondestructive Method for Probing Layer Thicknesses in Early Photographs From Micrometers to Nanometers Using SEM-Based  $\mu$ XRF Spectrometry," *Microscopy and Microanalysis* 30 (2024): 110–115.
21. M. S. Kozachuk, T. K. Sham, R. R. Martin, A. J. Nelson, I. Coulthard, and J. P. McElhone, "Recovery of Degraded-Beyond Recognition 19th Century Daguerreotypes With Rapid High Dynamic Range Elemental x-Ray Fluorescence Imaging of Mercury L Emission," *Scientific Reports* 8 (2018): 1–10.
22. B. Lavédrine, J.-P. Gandolfo, J. P. McElhone, and S. Monod, *Photographs of the Past: Process and Preservation* (Getty Conservation Institute, 2009).
23. M. S. Barger, S. V. Krishnaswamy, and R. Messier, "The Cleaning of Daguerreotypes: Comparison of Cleaning Methods," *Journal of the American Institute for Conservation* 22 (1982): 13–24.
24. S. Barger, A. Giri, W. White, and T. Edmondson, "Cleaning Daguerreotypes," *Studies in Conservation* 31 (1986): 15–28.
25. W. B. Wei, I. Gerritsen, and C. von Waldthausen, "Re-Examining the (Electro-) Chemical Cleaning of Daguerreotypes: Microscopic Change vs. Macroscopic Perception," *Topics in Photographic Preservation* 14 (2011): 24–40.
26. E. Grieten, O. Schalm, P. Tack, et al., "Reclaiming the Image of Daguerreotypes: Characterization of the Corroded Surface Before and After Atmospheric Plasma Treatment," *Journal of Cultural Heritage* 28 (2017): 56–64.
27. V. V. Golovlev, M. J. Gresalfi, J. C. Miller, et al., "Laser Characterization and Cleaning of 19th Century Daguerreotypes II," *Journal of Cultural Heritage* 4 (2003): 134–139.
28. E. M. Canosa, *Investigation and Optimization of Electrochemical Treatment for Daguerreotypes* (University of Arizona, 2016).
29. V. Ljubić Tobisch, K. Hradil, K. Whitmore, C. Strelí, P. Wobraschek, and W. Kautek, "Surface Characterization of Austrian Daguerreotype Portraits," *Journal of Cultural Heritage* 70 (2024): 223–230.
30. L. Bertrand, L. Robinet, M. Thoury, K. Janssens, S. X. Cohen, and S. Schöder, "Cultural Heritage and Archaeology Materials Studied by Synchrotron Spectroscopy and Imaging," *Applied Physics A: Materials Science & Processing* 106 (2012): 377–396.
31. M. S. Kozachuk, T.-K. Sham, R. R. Martin, A. Nelson, and I. Coulthard, "Eyeing the Past: Synchrotron m-XANES and XRF Imaging of Tarnish Distribution on 19th Century Daguerreotypes," *Journal of Synchrotron Radiation* 26 (2019): 1679–1686.
32. M. S. Kozachuk, T. K. Sham, R. R. Martin, et al., "Recovering Past Reflections: x-Ray Fluorescence Imaging of Electrocleaned 19th Century Daguerreotypes," *Heritage* 2 (2019): 568–586.
33. E. Da Silva, M. Robinson, C. Evans, A. Pejović-Milić, and D. V. Heyd, "Monitoring the Photographic Process, Degradation and Restoration of 21st Century Daguerreotypes by Wavelength-Dispersive x-Ray Fluorescence Spectrometry," *Journal of Analytical Atomic Spectrometry* 25 (2010): 654–661.

34. A. Shugar, K. Lough, and J. J. Chen, "Characterization of a Surface Tarnish Found on Daguerreotypes Revealed Under Shortwave Ultraviolet Radiation," *MRS Proceedings* 1656 (2014): 319–333, <https://doi.org/10.1557/opl.2014.706>.
35. P. Ravines, R. Wiegandt, and C. M. Wichern, "Surface Characterisation of Daguerreotypes With the Optical Metrological Technique of Confocal Microscopy," *Surface Engineering* 24 (2008): 138–146.
36. M. S. Kozachuk and J. P. McElhone, "Applying Nanoscience to Daguerreotypes: Understanding and Preserving the First Form of the Photograph/Appliquer la Nanoscience Aux daguerréotypes: Comprendre et préserver la première Forme de Photographie," *National Gallery of Canada Review* 9 (2018): 36–49.
37. A. E. Schlather, P. Gieri, M. Robinson, S. A. Centeno, and A. Manjavacas, "Nineteenth-Century Nanotechnology: The Plasmonic Properties of Daguerreotypes," *Proceedings of the National Academy of Sciences of the United States of America* 116 (2019): 13791–13798.
38. D. Ingerle, J. Swies, M. Iro, P. Wobrauschek, C. Strelt, and K. Hradil, "A Monochromatic Confocal Micro-x-Ray Fluorescence ( $\mu$ XRF) Spectrometer for the Lab," *Review of Scientific Instruments* 91 (2020): 1–8.
39. L. Brostoff, S. Zaleski, C. L. Ward-Bamford, et al., "Nineteenth Century Glass Manufacture and Its Effect on Photographic Glass Stability," *Journal of the Institute of Conservation* 43 (2020): 125–141.